

Online Supplement: About the Model

**Panayiota Poirazi,^{1,*} Terrence Brannon,²
and Bartlett W. Mel^{3,*}**

¹Institute of Molecular Biology and Biotechnology
Foundation for Research and
Technology, Hellas (FO.R.T.H.)
Vassilica Vouton
P.O. Box 1527
GR 711 10 Heraklion, Crete
Greece

²Metaperl IT Consulting
135 Corson Avenue

Staten Island, New York 10301

³Department of Biomedical Engineering and
Neuroscience Graduate Program
University of Southern California
Los Angeles, California 90089

*Correspondence: poirazi@imbb.forth.gr (P.P.), mel@usc.edu (B.W.M.)

In Section 1 of this supplement, we describe the process of constructing the pyramidal cell model. In Section 2, we show results of the validation studies used to calibrate the model based on data from published in vitro physiological studies. The parameters of the model are described in detail in Section 3.

1 Building the Model

Our goal was to construct and validate a state-of-the-art compartmental model of a CA1 pyramidal cell. Construction of the model was an immense project, as it involved adjusting the internal parameters of 17 types of ion channels, most of them distributed nonuniformly along the soma-dendritic axis, and 4 types of synaptic conductances. Constraints on the model arose from two main sources, including (1) data from studies primarily concerned with individual channel properties, including activation and inactivation curves, time constants, location-dependent channel densities, etc., and (2) data from studies primarily concerned with dendritic physiology and synaptic integration, including responses to current, voltage, and/or synaptic stimuli. In some cases, NEURON channel models developed by others were used with little or no modification, as detailed in Section 3. In spite of the complexity of the model as a whole, we were able through a lengthy manual iteration process to achieve good fits to a variety of experimental data, covering a broader range of phenomena than is handled by other pyramidal cell models that we know of. While we do not claim that the model is a perfect simulacrum of the real cell, its ability

to replicate many details relating to synaptic integration in the apical tree, with and without pharmacological blockers, contributes to our belief in the predictive value of our new simulation experiments which represent only minor modifications of existing methods.

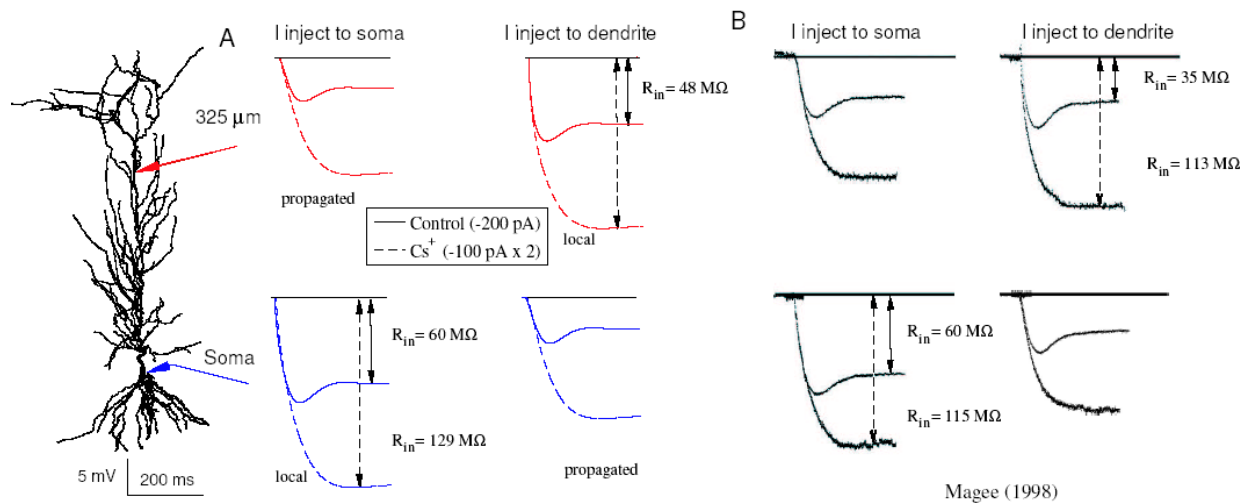
The model, available for download at <http://inc.usc.edu/CA1-pyramidal-cell-model>, could be improved in a number of ways. Dendritic spines could be explicitly modeled, an important change if issues relating to synaptic plasticity were to be addressed in future work. Spines were not included, as they can add significantly to the computational burden—depending on the number of compartments per spine and whether modeling of Ca^{++} machinery is included—and results of previous studies suggest that synaptic integration on the spatial scale of entire dendritic branches is not very sensitive to the presence or absence of dendritic spines. Spike shape in the soma and main apical trunk could also be improved through further tailoring of the various conductances involved. Spikes in the present model do not exhibit the smooth scoop-like repolarizations to the extent that is seen in typical slice recordings from CA1 pyramidal cells (e.g., Hoffman et al., 1997). Tailoring of spike shape is an arduous process, however, and we do not anticipate a significant change in model behavior as relates to synaptic integration. A more significant shortcoming of the model is the lack of attention paid to the channel composition of the basal dendrites, which were not directly stimulated in the present experiments. We do not therefore know if the cell's responses to stimulation of the basal dendrites will be either realistic or physiologically stable in its current state. However, this deficit could be remedied through a relatively straightforward “technology transfer” from the apical to the basal tree, subject to additional constraints from studies of basal dendritic physiology. The results of earlier modeling studies involving basal dendrites lead us to believe a similar form of synaptic integration may apply there as well (Mel, 1993; Mel et al., 1998; Archie and Mel, 2000).

2 Validation Studies

2.1 Effect of I_h on Input Resistance and Steady-State Voltage Propagation

The h-current, a hyperpolarization-activated mixed cation current, is responsible for the pronounced rectifying sag in response to a hyperpolarizing current pulse (Magee, 1998). The spatial distribution of I_h is highly nonuniform, with a 7-fold increase in channel density from the soma to the distal apical trunk. Though the apical trunk is of much smaller diameter than the soma, the huge resting conductance provided by the h-channels in the apical tree contributes to a lower input resistance measured distally than at the cell body and leads to an asymmetry in the distance-dependent attenuation of steady-state voltage signals—favoring voltage signals traveling inward from a dendritic stimulus to a recording electrode in the cell body (Magee, 1998).

Figure S1. Contribution of I_h to Input Resistance and Steady-State Voltage Propagation



(A) Following the methods of Magee (1998), a steady current was injected at either a somatic or dendritic electrode, and voltages were recorded at both locations. Responses are shown for somatic (left column) and dendritic (right column) current injections, under control conditions (-200 pA , solid curves) and with bath application of 3 mM Cs^+ (-100 pA , dashed curves), which we assumed blocked 80% of I_h (see Channel Blockers). Cs^+ traces were doubled in height in both (A) and (B) to allow more direct comparison of input resistances. R_{in} values are indicated in upper right and lower left panels, corresponding to measurements made at the site of current injection. Soma diameter was $8.6 \text{ }\mu\text{m}$, and dendritic diameter at recording site was $2.1 \text{ }\mu\text{m}$.

(B) Traces for same experiment, adapted with permission from Magee (1998).

We tested our model cell using constant hyperpolarizing current injections either at the soma or $325 \text{ }\mu\text{m}$ away in the main apical trunk and recorded at both sites simultaneously (Figure S1). We found voltage traces similar to those reported by Magee (1998), including (1) a pronounced depolarizing voltage sag, eliminated by blockade of I_h (dashed traces), (2) lower input resistance in the trunk compared to the cell body (averaging $50 \pm 3 \text{ M}\Omega$ distally versus $62 \pm 4 \text{ M}\Omega$ at the soma), and (3) asymmetric steady-state voltage attenuation favoring voltage signals propagating from the dendritic injection site to the cell body: we measured less decay—a 43% loss relative to the local dendritic response—for signals traveling to the soma, versus a 54% loss of the local somatic response for signals traveling $325 \text{ }\mu\text{m}$ into the dendrites. Magee reported a lower input resistance on average in the dendrites at this distance ($39 \pm 2 \text{ M}\Omega$) compared to the soma ($66 \pm 5 \text{ M}\Omega$), and related to this, an even milder attenuation for dendritic signals traveling inward (21% \pm 4% loss relative to original) compared to a 51% \pm 5% loss for somatic voltage signal traveling outward. Thus, our attenuation values, though greater than those reported by Magee, are less than those seen by others under similar in vitro conditions (Nace Golding, personal

communication). Differences of this magnitude can arise from variables that were not manipulated in this study, such as the diameter of the trunk and/or the number and diameter of side branches emerging from the trunk along the path to the soma. Furthermore, our dendritic measurements are always made with a “perfect seal,” which could bias our results to higher-than-experimental values for input resistance in dendritic recordings.

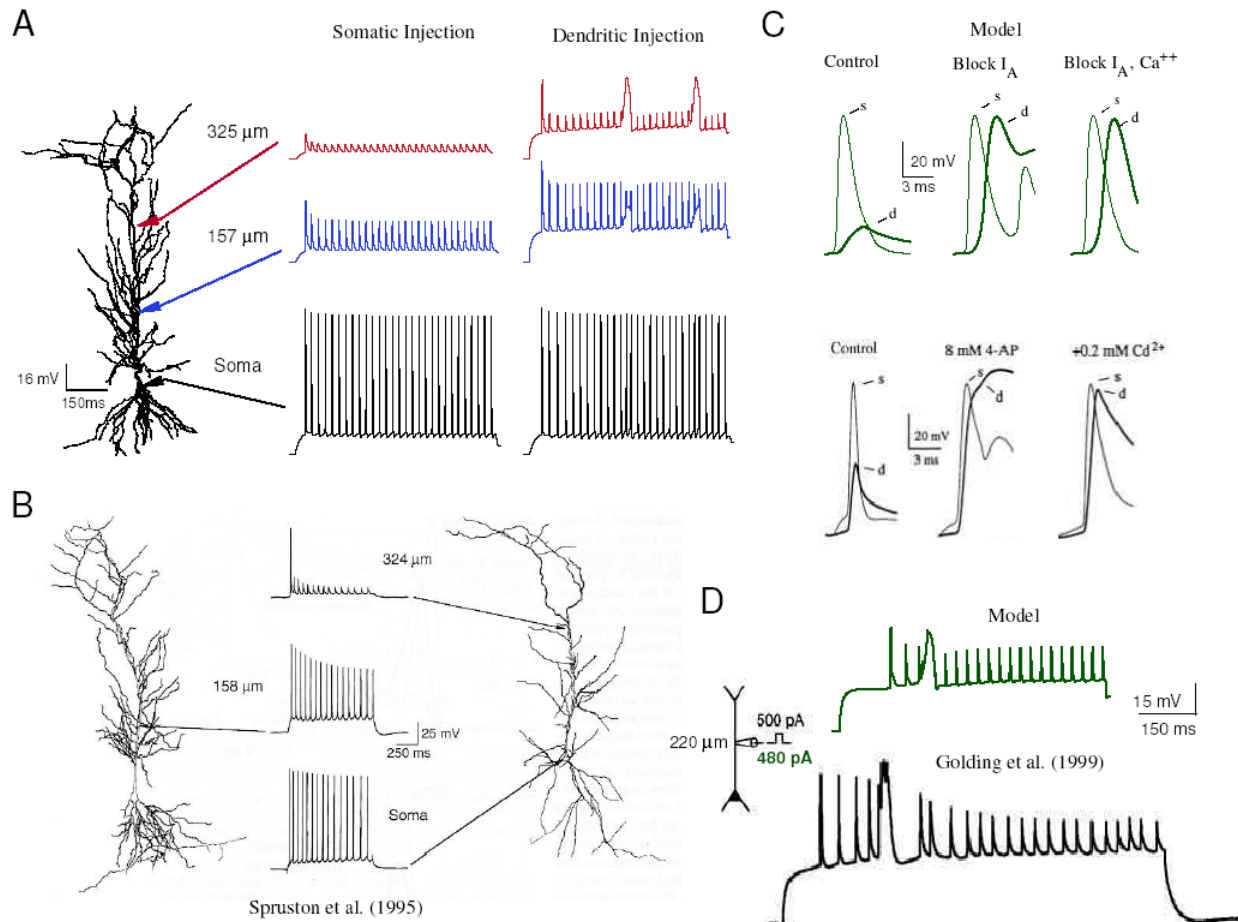
2.2 Properties of Backpropagating and Dendritically Initiated Action Potentials

A number of studies have examined the properties of back propagating action potentials (BPAPs) in the apical trunk (for review, see Stuart et al., 1997), including their tendency to attenuate with distance from the soma, and as a function of distance, their tendency to attenuate in the course of a spike train. The distance-dependent attenuation in CA1 pyramidal cells has been attributed to the 6-fold increase in the density of I_A in the apical trunk, a fast inactivating K^+ current that opposes transient depolarizations (Hoffman et al., 1997). The time-dependent attenuation, which is increasingly evident at greater distances from the cell body, has been attributed to slow inactivation of the Na^+ channel itself (Jung et al., 1997).

We tested our model cell using a constant depolarizing current injection at the soma while recording simultaneously at the soma and two locations in the apical trunk. We observed a pattern of distance and time-dependent attenuation of BPAPs (Figure S2A, “Somatic Injection”) similar to that reported by Spruston et al. (1995) (Figure S2B). One difference lay in the height of the first BPAP in the distal dendrite: high in the data of Spruston et al. (1995) and low in our traces. Interestingly, a subsequent study by Golding et al. (2001) found that CA1 pyramidal cells fall into two categories: those for which the first BPAP propagates at nearly full height into the distal dendrites, and those for which the first spike is reduced to a small spikelet by around 300 μm from the cell body. Thus, both types of responses are “normal.”

We repeated the experiment after blocking I_A throughout the cell and found that the initial BPAP now reached full height at the dendritic recording electrode as was also observed by Hoffman et al. (1997) (Figure S2C). Given that the cell is much more excitable in this condition than normal, the dendritic response in both data and model shows a failure to repolarize, as if the voltage were dominated by an unopposed dendritic Ca^{++} current. When calcium currents were 75% blocked to mimic bath application of 200 mM Cd^{++} , the dendritic spike, though broader than in control conditions, was more fully repolarized.

Figure S2. Properties of Action Potentials in the Apical Trunk



(A) Back-propagating action potentials elicited by steady somatic current injection (220 pA, 700 ms) show typical pattern of distance and time-dependent attenuation of spike height; results from Spruston et al. (1995) are reproduced with permission in (B) for comparison. Dendritic current injection (480 pA, 212 μm , 700 ms) leads to triggering of calcium spikes, large in the distal apical tree but seen at the cell body only as brief accelerations in spike rate.

(C) Initial somatic and dendritic spikes are shown in response to somatic current injection (300 pA, 50 ms) in control conditions (left), with block of I_A (middle), and with block of Ca^{++} currents (right). Results are comparable to those of Hoffman et al. (1997), reproduced with permission.

(D) Comparison of calcium spike elicited by dendritic current injection in model to data of Golding et al. (1999), reproduced with permission.

In another manifestation of the complex calcium-dependent physiology of pyramidal cell dendrites, it has been observed that Ca^{++} spikes can be evoked by direct dendritic stimulation, whereas activation of the distal dendrites by BPAPs initiated at the cell body rarely do so

(Amitai et al., 1993; Golding et al., 1999) unless, for example, coupled with synaptic input to the dendrites (Larkum et al., 1999). Golding et al (1999) found that the increased concentrations of Ca^{++} -dependent potassium currents near the cell body were primarily responsible for the active suppression of calcium spiking near the soma, a feature incorporated into the present model.

We tested our model to see if calcium spikes could be elicited in the apical tree in response to a direct dendritic current injection. The response of the cell to a 480 pA current injection at a distance of 212 μm is shown in Figure S2A (labelled “Dendritic Injection”) for the same three recording sites as before. The characteristic pattern of large amplitude slow spikes interrupting the regular train of fast spikes, with an initial onset delay of 200 ms or more, is similar to that reported by Golding et al (1999) under comparable stimulus conditions (Figure S2D).

Differences between our model and the data of Hoffman et al. (1997) include generally broader spikes in the model in both the soma and dendrites, somewhat less Ca^{++} excitability in the model cell after complete block of I_A , and a somewhat greater suppression of Ca^{++} channel-dependent excitability after 75% block of calcium channels. In addition, we observed a slow growth in spike height in our dendritic traces in response to dendritic current injection, compared to a slow decay in the traces of Golding et al (1999), due to a difference of unknown origin in the dynamics of the two cells. Overall, however, the model captures several major trends in spike shape and size as a function of location, time, injection site, and pharmacological manipulation.

2.3 Summary: Results of Validation Studies

The validation studies shown in Figures S1 and S2 indicate that our model provides reasonable fits to variety of in vitro data bearing on the biophysical and integrative properties of hippocampal CA1 pyramidal cells. The model exhibits (1) several I_h -dependent effects, including a realistic sag current, reasonable values for input resistance in the soma and dendrites, and the characteristic pattern of asymmetric voltage attenuation traveling to and from the cell body through the apical trunk, (2) a realistic pattern of distance and time-dependent attenuation in trains of back-propagating action potentials, with appropriate dependence on I_A , and (3) the elicitation of delayed-onset Ca^{++} spikes from a distal but not proximal stimulating electrode. In addition, Figures 1 and 2 in the accompanying paper (Poirazi et al., 2003) show that the model reproduces two different patterns of synaptic summation seen in different parts of the apical tree as reported by (Cash and Yuste, 1999), including the effects of pharmacological blockers.

3 The Compartmental Model

The compartmental model used in this work is a reconstruction of the CA1 pyramidal neuron shown in Figure S1 and was run with the NEURON simulation environment (Hines and Carnevale, 1997). The cell morphology is “n123” contained in Duke/Southampton archive of neuronal morphology at <http://www.cns.soton.ac.uk/~jchad/cellArchive/cellArchive.html>; see (Cannon et al. 1998). Since this cell morphology did not include an axon, we created one consisting of ten dendrite-like sections connected in series. The total length of the axon is 721 μm averaging 0.9 μm in diameter. We did not model nodes of Ranvier or myelination. The entire model consists of 183 compartments and includes a variety of active and passive membrane mechanisms known to be present in CA1 pyramidal cells. These include a leak current (I_{leak}), two

kinds of Hodgkin-Huxley-type sodium and potassium currents (somatic/axonic I_{Na}^{sa} and I_{Kdr}^{sa} , dendritic I_{Na}^d and I_{Kdr}^d), two A-type (proximal and distal) and one m-type potassium currents (I_A^p , I_m) a mixed conductance hyperpolarization-activated h-current (I_h), three types of voltage-dependent calcium currents, namely, a LVA T-type current (I_{CaT}), two HVAm R-type currents (somatic: I_{CaR}^s , dendritic: I_{CaR}^d), and two HVA L-type currents (somatic: I_{CaL}^s , dendritic: I_{CaL}^d), two types of Ca^{2+} -dependent potassium currents (a slow AHP current: I_{sAHP} ; and a medium AHP current: I_{mAHP}), a persistent sodium current (I_{pNa}), and four types of synaptic currents, namely, AMPA, NMDA, GABA_A, and GABA_B. Densities and distributions of the mechanisms included in our model are based on published empirical data as detailed below.

3.1 Nonuniform R_m

The efficacy of signal transduction within a neuron depends heavily on the membrane properties and internal resistivity of the dendritic arbor. Stuart and Spruston (1998) showed that while intracellular resistivity of layer 5 pyramidal neurons is low ($R_i \approx 65\text{--}100 \Omega cm$), voltage attenuation is substantial in these cells due to nonuniformity of the membrane resistance. The authors found that resting conductances in the distal dendrites have significant higher concentrations than in the proximal and somatic regions (up to a ratio of 36). Furthermore, they suggested that R_m follows a sigmoidally decreasing distribution from the soma to the distal trunk of pyramidal neurons. We implement a similar nonuniformity in our model, where the membrane resistance ($R_m = \frac{1}{g_{leak}}$) decreases sigmoidally from the soma to the apical trunk:

$$R_m(x) = R_{msoma} + \frac{(R_{mend} - R_{msoma})}{\left(1 + e^{\left(\frac{d_{half} - d_x}{steep}\right)}\right)} \quad (1)$$

where $R_{msoma} = 200 K\Omega cm^2$, $R_{mend} = 12 K\Omega cm^2$, $d_{half} = 200 \mu m$, $steep = 50 \mu m$, and d_x is the perpendicular distance of point x from the cell body. Based on these findings (Stuart and Spruston, 1998), and in order to replicate experimental data regarding signal attenuation, the axial model resistance also decreases sigmoidally from the soma to the apical trunk:

$$R_i(x) = R_{isoma} + \frac{(R_{iend} - R_{isoma})}{\left(1 + e^{\left(\frac{d_{half} - d_x}{steep}\right)}\right)} \quad (2)$$

where $R_{isoma} = 50 \Omega cm$, $R_{iend} = 35 \Omega cm$, $d_{half} = 210 \mu m$, $steep = 50 \mu m$. The axial resistance in all apical oblique and basal dendrites is set to the somatic value, i.e., $R_i = 50 \Omega cm$.

3.2 Standard Expression for Ionic Current

Our model cell contains a large variety of active currents which are expressed by the generic form

$$I_i = \bar{g}_i \cdot m^M \cdot h^N \cdot (V - E_i) \quad (3)$$

where \bar{g}_i is the maximal conductance of current I_i , and E_i is its reversal potential. The current activates according to M activation gates represented by the gating variable m . It inactivates with N inactivation gates represented by the variable h . h and m obey to first order kinetic equations.

3.3 Voltage-Dependent Sodium Current I_{Na} and Delayed Rectifier I_{Kdr}

The model kinetics for the Hodgkin-Huxley-like currents I_{Na} and I_{Kdr} are adapted originally from Bernanderet al. (1991). The sodium current is described by the equation

$$I_{Na} = \bar{g}_{Na} \cdot m^2 \cdot h \cdot s \cdot (V - E_{Na}) \quad (4)$$

where an additional variable s is introduced to account for dendritic location-dependent slow attenuation of the sodium current (Jung et al., 1997; Migliore et al., 1999). We use this parameter to vary the amount of attenuation along the apical trunk as a function of distance from the cell body such that proximal sections show little attenuation and distal sections show comparably more (with the exception of distal obliques, which show very little signal attenuation). Activation and inactivation kinetics for I_{Na} are given by

$$\begin{aligned} m_{t+dt} &= m_t + (1 - e^{-\frac{dt}{\tau_m}}) \cdot (m_{inf} - m_t) \\ h_{t+dt} &= h_t + (1 - e^{-\frac{dt}{\tau_h}}) \cdot (h_{inf} - h_t) \\ s_{t+dt} &= s_t + (1 - e^{-\frac{dt}{\tau_s}}) \cdot (s_{inf} - s_t) \end{aligned} \quad (5)$$

with $dt = 0.1$ ms and corresponding steady-state equations for m_{inf} , h_{inf} , and s_{inf} :

$$m_{inf} = \frac{1}{1 + e^{\left(-\frac{V+40}{3}\right)}}, h_{inf} = \frac{1}{1 + e^{\left(\frac{V+45}{3}\right)}}, s_{inf} = \frac{1 + Na_{att} \cdot e^{\left(\frac{V+60}{2}\right)}}{1 + e^{\left(\frac{V+60}{2}\right)}}, \quad (6)$$

and time constants $\tau_m = 0.05$ ms, $\tau_h = 0.5$ ms, and

$$\tau_\sigma = \frac{0.00333(ms) \cdot e^{0.0024(1/mV)} \cdot (V+60) \cdot Q(degC)}{1 + e^{0.0012(1/mV)} \cdot (V+60) \cdot Q(degC)} \quad (7)$$

The function $Q(degC)$ is given by

$$Q(degC) = \frac{F}{R \cdot (T + degC)} \quad (8)$$

where $R = 8.315$ joule/degC, $F = 9.648 \times 10^4$ Coul, $T = 273.16$ in degrees Kelvin, and $degC$ is the temperature in degrees celsius. The Na_{att} variable represents the degree of sodium current

attenuation and varies linearly from soma to distal trunk ($Na_{att} \in [0 \rightarrow 1]$: maximum \rightarrow zero attenuation).

Similarly, channel kinetics for the delayed rectifier current are given by

$$I_{Kdr} = \bar{g}_{Kdr} \cdot m^2 \cdot (V - E_K) \quad (9)$$

$$m_{t+dt} = m_t + (1 - e^{-\frac{dt}{2.2}}) \cdot (m_{inf} - m_t) \quad (10)$$

$$m_{inf} = \frac{1}{1 + e^{-\left(\frac{V+42}{2}\right)}} \quad (11)$$

The sodium and delayed rectifier channel properties are slightly different in the soma, axon, and dendritic arbor. To fit experimental data regarding the backpropagation of spike trains, soma and axon compartments have a lower threshold for Na^+ spike initiation ($\approx -57mV$) than dendritic ones ($\approx -50mV$). Thus, the m_{inf} and h_{inf} somatic/axonic HH channel kinetics as well as the time constants for both I_{Na}^{sa} and I_{Kdr}^{sa} are modified as follows. For the sodium channels,

$$m_{inf}^{sa} = \frac{1}{1 + e^{-\left(\frac{V+44}{3}\right)}}, h_{inf}^{sa} = \frac{1}{1 + e^{\left(\frac{V+49}{3.5}\right)}}, \quad (12)$$

while the new m_{inf} for the delayed rectifier is

$$m_{inf}^{sa} = \frac{1}{1 + e^{-\left(\frac{V+46.3}{3}\right)}} \quad (13)$$

The somatic time constant for somatic/axonic Na^+ channel activation is kept the same $\tau_{hh}^a = 0.05$ ms while for inactivation is set to $\tau_h^a = 1$ ms while the τ value for the delayed rectifier channel activation is set to $\tau_m^a = 3.5$ ms. In all of the following equations, τ values in expressions of the form $e^{-\frac{dt}{\tau}}$ are given in ms, while in functions with V as an input, the symbol V is in mV.

Conductance values for all HH mechanisms are shown in the following table:

$$\begin{array}{ll} \text{Soma:} & \bar{g}_{Na}^s = 7mS/cm^2, \quad \bar{g}_{Kdr}^s = 1.4mS/cm^2 \\ \text{Axon:} & \bar{g}_{Na}^a = 100mS/cm^2, \quad \bar{g}_{Kdr}^a = 20mS/cm^2 \\ \text{Other compartments:} & \bar{g}_{Na}^d = 7mS/cm^2, \quad \bar{g}_{Kdr}^d = 0.867mS/cm^2 \end{array} \quad (14)$$

3.4 Fast Inactivating Potassium Current I_A

A-type potassium channels are known to be distributed in high densities in the dendrites of CA1 pyramidal neurons while channel kinetics appear to differ between proximal and distal populations. Furthermore, the density of these channels was found to increase by more than a factor of 6 from the soma to 350 μm in the apical trunk (Hoffman et al., 1997; Migliore et al., 1999). Based on these findings, we implement a linear increase in I_A channel conductance along the apical trunk, with different channel kinetics for proximal (I_{Aprox}) versus distal ($I_{A,dist}$) compartments, as per Hoffman et al. (1997). Kinetic equations for both channels are given by

$$I_A = \bar{g}_A \cdot m \cdot h \cdot (V - E_K) \quad (15)$$

$$m_{t+dt} = m_t + (1 - e^{-\frac{dt}{\tau_m}}) \cdot \left(\frac{1}{1 + \alpha_m(V)} - m_t \right),$$

$$h_{t+dt} = h_t + (1 - e^{-\frac{dt}{\tau_h}}) \cdot \left(\frac{1}{1 + \alpha_h(V)} - h_t \right), \quad (16)$$

with $\alpha(V)$, $\beta(V)$ equations and time constants (in ms) for the proximal I_A given by

$$\alpha_m(V) = e^{(10^{-3} \cdot \zeta(V) \cdot (V-11) \cdot Q(\text{degC}))}, \beta_m(V) = e^{(0.00055 \cdot \zeta(V) \cdot (V-11) \cdot Q(\text{degC}))} \quad (17)$$

$$\alpha_h(V) = e^{(0.003 \cdot (V+56) \cdot Q(\text{degC}))}, \beta_h(V) = \alpha_h(V) \quad (18)$$

$$\tau_m = \max\left(\frac{\beta_m(V)}{0.05(1/\text{ms}) \cdot qt(\text{degC}) \cdot (1 + \alpha_m(V))}, 0.1\right),$$

$$\tau_h = \max(0.26(\text{ms/mV}) \cdot (V+50), 2) \quad (19)$$

where the functions $\zeta(V)$ and $qt(\text{degC})$ are

$$\zeta(V) = -1.5 - \frac{1}{1 + e^{(V+40)/5}} (1/\text{mV}), qt(\text{degC}) = 5 \frac{(\text{degC} - 24)(C^\circ)}{10(C^\circ)}, \quad (20)$$

Corresponding equations for $\alpha(V)$'s, $\beta(V)$'s and τ 's for distal channels are given by

$$\alpha_m(V) = e^{(10^{-3} \cdot \zeta(V) \cdot (V+1) \cdot Q(\text{degC}))}, \beta_m(V) = e^{(0.00039 \cdot \zeta(V) \cdot (V+1) \cdot Q(\text{degC}))} \quad (21)$$

$$\alpha_h(V) = e^{(0.003 \cdot (V+56) \cdot Q(\text{degC}))}, \beta_h(V) = \alpha_h(V) \quad (22)$$

$$\tau_m = \max\left(\frac{\beta_m(V)}{(0.1 \cdot qt(degC) \cdot (1 + \alpha_m(V)))}, 0.1\right),$$

$$\tau_h = \max(0.26(ms/mV) \cdot (V + 50), 2) \quad (23)$$

with function $\zeta(V)$ expressed as

$$\zeta(V) = -1.8 - \frac{1}{1 + e^{(V+40)/5}}(1/mV) \quad (24)$$

The maximal conductance values for both channel types vary as a function of distance from the cell body according to the following equations:

$$\bar{g}_{Aprox}(x) = \begin{cases} g_{Asoma} & \text{if } d_x \leq 100\mu m \\ 0 & \text{if } d_x > 100\mu m \end{cases} \quad (25)$$

$$\bar{g}_{Adist}(x) = \begin{cases} 0 & \text{if } d_x \leq 100\mu m \\ \bar{g}_{Ainit} \cdot \bar{g}_{Afactor} \cdot \frac{d_x}{350\mu m} & \text{if } 100 < d_x \leq 350\mu m \\ \bar{g}_{Ainit} \cdot \bar{g}_{Afactor} & \text{if } d_x > 350\mu m \end{cases} \quad (26)$$

where the somatic conductance $\bar{g}_{Asoma} = 7.5mS/cm^2$, the initial conductance value $\bar{g}_{Ainit} = 7.488mS/cm^2$, and the maximum dendritic factor $\bar{g}_{Afactor} = 6.5$. The above trunk distribution results in more than 5-fold increase in the A-current conductance at 300 μm , similar to the experimental value reported by Hoffman et al. (1997).

3.5 Hyperpolarization Activated Current I_h

The hyperpolarization-activated h-current is known to be differentially distributed along the dendritic arbor of CA1 neurons with increasing channel density from the soma to the distal trunk sections (Magee, 1998). The elevated dendritic conductance has been shown to have a location-dependent impact in the basic membrane properties and the propagation of voltage traces (Magee, 1998). In order to fit these empirical data, the I_h mechanism in our model cell is distributed in a sigmoidally increasing manner from the soma to the main apical trunk:

$$\bar{g}_h(x) = \bar{g}_{hsoma} + \frac{\bar{g}_{hend} - \bar{g}_{hsoma}}{1 + e^{\left(\frac{d_{half} - d_x}{steep}\right)}} \quad (27)$$

where $\bar{g}_{hsoma} = 18.72mS/cm^2$, $\bar{g}_{hend} = 9 \cdot \bar{g}_{hsoma}$, $d_{half} = 280\mu m$, $steep = 50\mu m$. This implementation results in a 7-fold increase in I_h conductance at 350 μm as per (Magee, 1998).

The kinetic equations for h-type channels are given by

$$I_h = \bar{g}_h \cdot m \cdot (V - E_h) \quad (28)$$

where $E_h = -10\text{mV}$ is the h-current reversal potential.

$$\frac{dm}{dt} = \frac{1 - \left(\frac{1}{1 + e^{-(V+90)/8.5}} \right) - m}{\tau} \quad (29)$$

$$\tau = \begin{cases} 1 & \text{if } V > -30\text{mV} \\ \frac{2}{(e^{-((V+145)/17.5)} + e^{((V+16.8)/16.5)})} + 10 & \text{otherwise} \end{cases} \quad (30)$$

3.6 Voltage-Dependent Calcium Currents

Calcium channel kinetic equations and density distributions are adapted from Magee and Johnston (1995) and were modified to account for distally evoked Ca^{++} spikes. LVA (T-type) Ca^{++} channel kinetics are given by

$$I_{\text{CaT}} = \bar{g}_{\text{CaT}} \cdot m^2 \cdot h \cdot \frac{0.001\text{mM}}{0.001\text{mM} + ca_{in}} \cdot ghk(V, ca_{in}, ca_{out}) \quad (31)$$

$$ghk(V, ca_{in}, ca_{out}) = -x \cdot \left(1 - \frac{ca_{in}}{ca_{out}} \cdot e^{\frac{V}{x}} \right) \cdot f\left(\frac{V}{x}\right) \quad (32)$$

$$x = \frac{0.0853 \cdot (T + \text{degC})}{2}, f(z) = \begin{cases} 1 - \frac{z}{2} & \text{if } \text{abs}(z) < 10^{-4} \\ \frac{z}{e^z - 1} & \text{otherwise} \end{cases} \quad (33)$$

$$\begin{aligned} m_{t+dt} &= m_t + \left(1 - e^{-\frac{dt}{\tau_m}} \right) \cdot \left(\frac{\alpha_m(V)}{\alpha_m(V) + \beta_m(V)} - m_t \right), \\ h_{t+dt} &= h_t + \left(1 - e^{-\frac{dt}{\tau_h}} \right) \cdot \left(\frac{\alpha_h(V)}{\alpha_h(V) + \beta_h(V)} - h_t \right), \end{aligned} \quad (34)$$

where ca_{in} and ca_{out} are the internal and external calcium concentrations. $\alpha(V)$ s', $\beta(V)$ s', and τ s' are given by

$$\alpha_m(V) = -0.196 \cdot \frac{(V - 19.88)}{e^{-(V-19.88)/10} - 1}, \beta_m(V) = 0.046 \cdot e^{-(V/22.73)} \quad (35)$$

$$\alpha_h(V) = 0.00016 \cdot e^{-(V+57)/19}, \beta_h(V) = \frac{1}{e^{-(V-15)/10} + 1} \quad (36)$$

$$\tau_m = \frac{1}{\alpha_m(V) + \beta_m(V)}, \tau_h = \frac{1}{0.68 \cdot (\alpha_h(V) + \beta_h(V))} \quad (37)$$

LVA (T-type), Ca^{++} channels are distributed along the main trunk, starting from the proximal dendrites to the distal tuft, with linearly increasing conductance as shown by

$$\bar{g}_{CaT}(x) = \begin{cases} 0 & \text{if } d_x < 100\mu\text{m} \\ \bar{g}_{CaT_{init}} \cdot \bar{g}_{CaT_{factor}} \cdot \frac{d_x}{350\mu\text{m}} & \text{if } d_x \geq 100\mu\text{m} \end{cases} \quad (38)$$

where $\bar{g}_{CaT_{init}} = 0.1\text{mS/cm}^2$ and $\bar{g}_{CaT_{factor}} = 4$. LVA (T-type), Ca^{++} channels are also inserted at the soma with a conductance value of $\bar{g}_{CaT_{soma}} = 0.05\text{mS/cm}^2$.

The dendritic HVAm (R-type) Ca^{++} channels are distributed in a uniform way along the apical trunk, with a small conductance value of $\bar{g}_{CaR}^d = 0.3\text{mS/cm}^2$. The corresponding somatic conductance is ten times higher than the apical trunk value, $\bar{g}_{CaR}^s = 3\text{mS/cm}^2$. Channel kinetics are given by the equations

$$I_{CaR} = \bar{g}_{CaR} \cdot m^3 \cdot h \cdot (V - E_{Ca}) \quad (39)$$

$$m_{t+dt} = m_t + (1 - e^{-\frac{dt}{\tau_m}}) \cdot (\alpha(V) - m_t), \quad h_{t+dt} = h_t + (1 - e^{-\frac{dt}{\tau_h}}) \cdot (\beta(V) - h_t), \quad (40)$$

The difference between somatic and dendritic CaR currents lies in the $\alpha(V)$, $\beta(V)$, and τ parameter values. For the somatic current, $\tau_m = 100$ ms and $\tau_h = 5$ ms, while for the dendritic current, $\tau_m = 50$ ms and $\tau_h = 5$ ms. The $\alpha(V)$ and $\beta(V)$ equations for dendritic CaR channels are

$$\alpha(V) = \frac{1}{1 + e^{-(v+48.5)/3}}, \quad \beta(V) = \frac{1}{1 + e^{(v+53)}} \quad (41)$$

while for somatic CaR channels

$$\alpha(V) = \frac{1}{1 + e^{-(v+60)/3}}, \quad \beta(V) = \frac{1}{1 + e^{(v+62)}} \quad (42)$$

Most of the kinetic equations for somatic HVA (L-type) channels are the same as equations for T-type channels. Equations that are different between the two mechanisms are given by

$$I_{CaL}^s = \bar{g}_{CaL}^s \cdot m \cdot \frac{0.001mM}{0.001mM + ca_{in}} \cdot ghk(V, ca_{in}, ca_{out}) \quad (43)$$

$$\alpha_m(V) = -0.055 \cdot \frac{(V+27.01)}{e^{-(V+27.01)/3.8} - 1}, \quad \beta_m(V) = 0.94 \cdot e^{-(V+63.01)/17} \quad (44)$$

$$\tau_m = \frac{1}{5 \cdot (\alpha_m(V) + \beta_m(V))} \quad (45)$$

Most of the kinetic equations for our dendritic HVA (L-type) channels are the same as the equations for the R-type channels. Equations that are different between the two mechanisms are given by

$$I_{CaL}^d = \bar{g}_{CaL}^d \cdot m^3 \cdot h \cdot (V - E_{Ca}) \quad (46)$$

$$\alpha(V) = \frac{1}{1 + e^{-(v+37)}}, \beta(V) = \frac{1}{1 + e^{(v+41)/0.5}} \quad (47)$$

with time constants equal to $\tau_m = 3.6$ ms and $\tau_h = 29$ ms.

The dendritic HVA (L-type) channels are distributed in a nonuniform way along the apical trunk:

$$\bar{g}_{CaL}^d(x) = \begin{cases} 0.1 \cdot \bar{g}_{CaL_{init}} & \text{if } d_x < 50 \mu m \\ 4.6 \cdot \bar{g}_{CaL_{init}} & \text{if } d_x \geq 50 \mu m \end{cases} \quad (48)$$

where $\bar{g}_{CaL_{init}} = 0.316 \text{ mS/cm}^2$ and the corresponding somatic conductance is equal to $\bar{g}_{CaL}^s = 7 \text{ mS/cm}^2$. No Ca^{++} channels were inserted in the axon or the basal dendrites of our model.

3.7 Calcium Pumping/Buffering

A calcium pump/buffering mechanism is also inserted at the cell body and along the apical trunk. The mechanism is taken from Destexhe et al. (1994) and was modified to replicate the sharp Ca^{++} spike repolarization observed in Golding et al. (1999). The factor for Ca^{++} entry was changed from $f_e = 10,000$ to $f_e = 10,000/18$, and the rate of calcium removal was made seven times faster. The kinetic equations are given by

$$drive_{channel} = \begin{cases} -f_e \cdot \frac{I_{Ca}}{0.2 \cdot FARADAY} & \text{if } drive_{channel} > 0 \text{ mM/ms} \\ 0 & \text{otherwise} \end{cases} \quad (49)$$

$$\frac{dca}{dt} = drive_{channel} + \frac{(10^{-4}(\text{mM}) - ca)}{7 \cdot 200(\text{ms})} \quad (50)$$

3.8 Calcium-Dependent Potassium Current I_{AHP}

Empirical data suggest that the excitatory effects of calcium channels in the soma and proximal trunk regions are counteracted by Ca^{++} -activated potassium channels (Sah and Bekkers, 1996). Thus, Ca^{++} -dependent slow and medium AHP potassium channels (along with a calcium pump/buffering mechanism) are distributed in a higher conductance along these regions:

$$\bar{g}_{sAHP}(x) = \begin{cases} 5 \cdot \bar{g}_{sAHP_{init}} & \text{if } 50 < d_x < 200 \mu m \\ 0.5 \cdot \bar{g}_{sAHP_{init}} & \text{otherwise} \end{cases} \quad (51)$$

$$\bar{g}_{mAHP}(x) = \begin{cases} 2 \cdot \bar{g}_{mAHP_{init}} & \text{if } 50 < d_x < 200 \mu m \\ 0.25 \cdot \bar{g}_{mAHP_{init}} & \text{otherwise} \end{cases} \quad (52)$$

where $\bar{g}_{sAHP_{init}} = 0.1 \text{ mS/cm}^2$ and $\bar{g}_{mAHP_{init}} = 16.5 \text{ mS/cm}^2$. The somatic values for these two channels are equal to $\bar{g}_{sAHP_{soma}} = 0.5 \text{ mS/cm}^2$ and $\bar{g}_{mAHP_{soma}} = 90.75 \text{ mS/cm}^2$.

The channel kinetics for I_{sAHP} are taken with no modifications from Destexhe et al. (1994), and the kinetics equations are given by

$$I_{sAHP} = \bar{g}_{sAHP} \cdot m^3 \cdot (V - E_K) \quad (53)$$

$$\frac{dm}{dt} = \frac{\frac{Cac}{1 + Cac} - m}{\tau} \quad (54)$$

$$\tau = \max\left(\frac{1}{0.003(1/ms) \cdot (1 + Cac) \cdot 3^{(degC-22)/10}}, 0.5\right) \quad (55)$$

where $Cac = (ca_{in}/0.025 \text{ (mM)})^2$.

The medium AHP current I_{mAHP} taken from Moczydlowski and Latorre (1983) is given by

$$I_{mAHP} = \bar{g}_{mAHP} \cdot m \cdot (V - E_K) \quad (56)$$

$$m_{t+dt} = m_t + (1 - e^{-\frac{dt}{\tau_m}}) \cdot \left(\frac{\alpha_m(V)}{\tau_m} - m_t\right) \quad (57)$$

$$\alpha_m(V) = \frac{0.48(1/ms)}{1 + \frac{0.18(mM)}{ca_{in}} \cdot e^{(-1.68 \cdot V \cdot Q(degC))}},$$

$$\beta_m(V) = \frac{0.28(1/ms)}{1 + \frac{ca_{in}}{0.011(mM)} \cdot e^{(-2 \cdot V \cdot Q(degC))}} \quad (58)$$

$$\tau_m = \frac{1}{\alpha_m(V) + \beta_m(V)} \quad (59)$$

3.9 Slowly Inactivating Potassium Current I_m

A slowly activating voltage-dependent potassium current (I_m) is inserted along the apical trunk and cell body with a fixed conductance value $\bar{g}_{km} = 60 \text{ mS/cm}^2$, with the exception of oblique side branches where $\bar{g}_{km} = 120 \text{ mS/cm}^2$. The channel is given by the equations

$$I_m = 10^{-4} \cdot T_{adj}(degC) \cdot \bar{g}_m \cdot m \cdot (V - E_K) \quad (60)$$

$$T_{adj}(degC) = 2.3^{(degC-23)/10} \quad (61)$$

$$m_{t+dt} = m_t + (1 - e^{-\frac{dt \cdot T_{adj}(degC)}{\tau}}) \cdot \left(\frac{\alpha(V)}{\alpha(V) + \beta(V)} - m_t\right) \quad (62)$$

$$\alpha(V) = 10^{-3} \cdot \frac{(V+30)}{(1 - e^{-(V+30)/9})}, \beta(V) = -10^{-3} \cdot \frac{(V+30)}{(1 - e^{-(V+30)/9})} \quad (63)$$

$$\tau = \frac{1}{\alpha(V) + \beta(V)} \quad (64)$$

Finally, a persistent sodium channel is inserted in the distal apical tuft. The channel is described by the equations

$$I_{Nap} = \bar{g}_{Nap} \cdot m^3 \cdot (V - E_{Na}) \quad (65)$$

where

$$m = \frac{1}{(1 + e^{-(V+50.4)/4.5})} \quad (66)$$

In addition to the above channel mechanisms, AMPA, NMDA, GABA_A, and GABA_B synaptic mechanisms are implemented in the model. These were taken from Destexhe et al. (1997) without modification.

Due to the lack of empirical data bearing on the densities and distribution of conductances within oblique side branches, most channel properties in our model are set to be identical for all branches extending from the main apical trunk, after an initial section. Membrane properties for oblique sections within 50 μm from the trunk follow the respective trunk values, while most conductance values beyond the first 50 μm are set equal to the values in a selected trunk section located at 157 μm from the cell body. Specifically, conductance values are distributed as follows:

$$\bar{g}_{all}(x) = \begin{cases} \bar{g}_{all_{trunk}} & \text{if } d(x, trunk) \leq 50 \\ \bar{g}_{all_{hold}} & \text{if } d(x, trunk) > 50 \text{ and } d_x < 300 \mu\text{m} \end{cases} \quad (67)$$

where \bar{g}_{all} includes conductance values for I_A ($\bar{g}_{Aprox_{hold}} = 0$, $g_{Adist_{hold}} = 27.285 \text{ mS/cm}^2$), I_h

($g_{h_{hold}} = 30.5 \text{ mS/cm}^2$), \bar{g}_{leak} ($g_{leak_{hold}} = 6.94 \times 10^{-6} \text{ I}/\Omega\text{cm}^2$), I_{CaR}^d ($g_{CaR_{hold}}^d = 0.03 \text{ mS/cm}^2$), I_{CaL}^d ($g_{CaL_{hold}}^d = 1.455 \text{ mS/cm}^2$), I_{CaT} ($g_{CaT_{hold}} = 0.179 \text{ mS/cm}^2$), I_{sAHP} ($g_{sAHP_{hold}} = 0.5 \text{ mS/cm}^2$), I_{mAHP} ($g_{mAHP_{hold}} = 18.5 \text{ mS/cm}^2$), I_m ($g_{Km_{hold}} = 60 \text{ mS/cm}^2$), and I_{pNa} ($g_{pNa_{trunk}} = 5.6 \times 10^{-5} \text{ mS/cm}^2$, $g_{pNa_{hold}} = 0.00028 \text{ mS/cm}^2$) (inserted only in oblique dendrites). The Na^+ spike attenuation variable

Na^{att} also follows the above rules. The parameter $\bar{g}_{all_{trunk}}$ refers to the respective trunk values for all conductances within each oblique, while $\bar{g}_{all_{hold}}$ denotes the selected conductance values taken from the trunk section at 157 μm . The function $d(x, trunk)$ measures the path distance from any point x in the oblique to the connection side with the trunk.

For oblique dendrites located beyond 300 μm (vertical distance from soma), channel conductances are modified as follows to account for distally evoked Ca^{++} spikes:

$$\begin{aligned}
\bar{g}_{Adist}(x) &= 2.47 \cdot \bar{g}_{Adist_{hold}} & \text{if } d_x > 300 \mu m \\
\bar{g}_{CaR}^d(x) &= 13 \cdot g_{CaR_{hold}^d} & \text{if } d_x > 300 \mu m \\
\bar{g}_{sAHP}(x) &= 5 \cdot \bar{g}_{sAHP_{init}} & \text{if } d_x > 300 \mu m \\
g_{Kdr}^d(x) &= 1.07 \cdot g_{Kdr_{hold}^d} & \text{if } d_x > 300 \mu m \\
\bar{g}_{pNa}(x) &= 2 \cdot \bar{g}_{pNa_{hold}} & \text{if } d_x > 350 \mu m \\
Na_{att}(x) &= 0.95 & \text{if } d_x > 350 \mu m
\end{aligned} \tag{68}$$

$$\begin{aligned}
\bar{g}_{CaL}^d(x) &= 14 \cdot g_{CaL_{hold}^d} & \text{if } 300 < d_x \leq 350 \mu m \\
&= 15 \cdot g_{CaL_{hold}^d} & \text{if } d_x > 350 \mu m
\end{aligned} \tag{69}$$

To account for the activity-dependent attenuation of sodium channel conductance in CA1 cells, we vary the amount of attenuation along the apical trunk of our model as a function of distance from the cell body such that proximal sections show little attenuation and distal sections show comparably more. We implement a linear decay from proximal to distal dendrites with an exception in the distal oblique dendrites where the sodium channel attenuation is very small ($Na_{att} = 0.95$ for $d_x > 300 \mu m$).

The basal dendrites of our model contain significantly fewer membrane mechanisms since the focus of the current work is to study synaptic integration in apical oblique dendrites. To define basal conductance values in addition to the HH mechanisms, we select (hold) the conductance values at an apical trunk section located at $50 \mu m$ from the cell body and use the following equations:

$$\begin{aligned}
\bar{g}_{Adist}(x) &= 1.6 \cdot \bar{g}_{Adist_{hold}} \\
\bar{g}_{Aprox}(x) &= 1.6 \cdot \bar{g}_{Aprox_{hold}} \\
R_m(x) &= R_{m_{hold}} \\
\bar{g}_h(x) &= \bar{g}_{h_{soma}}
\end{aligned} \tag{70}$$

The AMPA and NMDA conductance values are estimated such that a single pulse depolarization delivered at any location along the apical tree will give rise to a 5mV local EPSP. Therefore, the AMPA and NMDA conductances vary with location, but the ratio between the two is constant within a dendritic subregion. In the trunk and soma, the NMDA/AMPA ratio is 0.6, while in oblique dendrites the ratio is 2.5. These values were set in order to match the effects of NMDA channel blockade reported by Cash and Yuste (1999), as shown in Figures 1 and 2 of Poirazi et al. (2003).

The GABA_A and GABA_B kinetic model implementation followed Destexhe et al. (1994) and Destexhe et al. (1997). For the experiments reported in Figure 4 of Poirazi et al. (2003), we use a

uniform distribution of both GABA_A and GABA_B receptors along the entire model, where each compartment activated by a single high-frequency stimulus delivered at a group of synapses receives one GABA_A and one GABA_B inhibitory input. The GABA_A conductance is set to 100% the local AMPA conductance value and GABA_B conductance set equal to 60% the GABA_A value.

Passive biophysical parameters of the model are as follows: R_m and R_i are sigmoidally changing along the apical trunk (see above), $C_m = 1 \mu\text{F}/\text{cm}^2$, the temperature used in all experiments is 34°C, and the reversal potentials are set to $E_{Na} = 50\text{mV}$, $E_K = -80\text{mV}$, $E_h = -10\text{mV}$, $E_{Ca} = 140\text{mV}$. The reversal potential for the passive model conductance, E_{leak} , is calculated so that the membrane potential at rest is equal to -70mV everywhere.

No additional manipulations were made to account for spines in this model.

3.10 Channel Blockers

We simulate the effect of various channel blockers based on experimental data regarding the selectivity/affinity and effectiveness of each drug.

Nickel (Ni^{2+}) is the most commonly used antagonist for T-type calcium channels due to its selectivity when used in small doses (10–50 μM). However, there is evidence that in hippocampal neurons larger amounts of this drug may inhibit other calcium channel types (Ozawa et al., 1989; Avery and Johnston, 1998). Thus, when modeling the effects of bath application of 1 mM Ni^{2+} , we assume that due to the very high blocker concentration, all Ca^{++} channels are completely blocked.

Cadmium (Cd^{2+}) is a nonselective Ca^{++} channel blocker at high concentrations. However, at lower concentrations, LVA currents have shown less susceptible to the drug than HVA currents (Ozawa et al., 1989), though this effect is dose dependent and may depend strongly on the membrane potential at the time of the application (Avery and Johnston, 1998). In our model, we simulate the effects of 200 μM Cd^{2+} bath application by a 75% blockade of all Ca^{++} channels.

Cesium (Cs^+) is known to selectively block h-current in hippocampal neurons. As reported by Magee (1998), bath application of 3 mM Cs^+ results in the blockade of $\approx 80\%$ of I_h . Thus, we model this blocker effect by a corresponding 80% channel blockade.

4-Aminopyridine (4-AP) is a widely used blocker for the transient K^+ channels, and its effectiveness in CA1 neurons has been found to be dose dependent (Hoffman et al., 1997). In our model, we simulate the effects of 3 mM 4-AP bath application with 80% block of A-current, a value somewhat higher than reported (estimated 50% channel blockage at 1.4 mM of 4-AP). We assume that 8 mM of 4-AP result in a 100% channel blockade.

When simulating blocker application for Na^+ channels and NMDA receptors in our model, these currents were always blocked completely, since the experimental concentrations of TTX (5 μM) and AP-5 (100 μM) were accordingly high.

Supplemental References

- Amitai, Y., Friedman, A., Connors, B., and Gutnick, M. (1993). Regenerative electrical activity in apical dendrites of pyramidal cells in neocortex. *Cereb. Cortex* 3, 26–38.
- Archie, K.A., and Mel, B.W. (2000). An intradendritic model for computation of binocular disparity. *Nat. Neurosci.* 3, 54–63.
- Avery, R.B., and Johnston, D. (1998). Multiple channel types contribute to the low-voltage activated current in hippocampal CA3 pyramidal neurons. *J. Neurosci.* 16, 5567–5582.
- Bernander, O., Douglas, R., Martin, K., and Koch, C. (1991). Synaptic background activity influences spatiotemporal integration in single pyramidal cells. *Proc. Natl. Acad. Sci. USA* 88, 11569–11573.
- Cash, S., and Yuste, R. (1999). Linear summation of excitatory inputs by CA1 pyramidal Neurons. *Neuron* 22, 383–394.
- Destexhe, A., Mainen, Z., and Sejnowski, T. (1994). Synthesis of models for excitable membranes, synaptic transmission and neuromodulation using a common kinetic formalism. *J. Comput. Neurosci.* 1, 195–230.
- Destexhe, A., Mainen, Z.F., and Sejnowski, T.J. (1997). Kinetic models of synaptic transmission. In *Methods in Neuronal Modeling, Second Edition*, C. Koch and I. Segev, Eds. (Cambridge, MA: MIT Press).
- Golding, N.L., Jung, H.-Y., Mickus, T., and Spruston, N. (1999). Dendritic calcium spike initiation and repolarization are controlled by distinct potassium channel subtypes in CA1 pyramidal neurons. *J. Neurosci.* 19, 8789–8798.
- Golding, N.L., Kath, W.L., and Spruston, N. (2001). Dichotomy of action-potential backpropagation in CA1 pyramidal neuron dendrites. *J Neurophysiol.* 86, 2998–3010.
- Hines, M.L., and Carnevale, N.T. (1997). The NEURON simulation environment. *Neural Comput.* 9, 1179–1209.
- Hoffman, D.A., Magee, J.C., Colbert, C.M., and Johnston, D. (1997). K⁺ channel regulation of signal propagation in dendrites of hippocampal pyramidal neurons. *Nature* 387, 869–875.
- Jung, H.-Y., Mickus, T., and Spruston, N. (1997). Prolonged sodium channel inactivation contributes to dendritic action potential attenuation in hippocampal pyramidal neurons. *J. Neurosci.* 17, 6639–6647.
- Larkum, M.E., Zhu, J.J., and Sakmann, B. (1999). A new cellular mechanism for coupling inputs arriving at different cortical layers. *Nature* 398, 338–341.
- Magee, J.C. (1998). Dendritic hyperpolarization-activated currents modify the integrative properties of hippocampal CA1 pyramidal neurons. *J. Neurosci.* 18, 7613–7624.
- Magee, J.C., and Johnston, D. (1995). Synaptic activation of voltage-gated channels in the dendrites of hippocampal pyramidal neurons. *Science* 268, 301–304.
- Mel, B.W. (1993). Synaptic integration in an excitable dendritic tree. *J. Neurophysiol.* 70, 1086–1101.

- Mel, B.W., Ruderman, D.L., and Archie, K.A. (1998). Translation-invariant orientation tuning in visual 'complex' cells could derive from intradendritic computations. *J. Neurosci.* *17*, 4325–4334.
- Migliore, M., Hoffman, D., Magee, J., and Johnston, D. (1999). Role of an A-type K^+ conductance in the back-propagation of action potentials in the dendrites of hippocampal pyramidal neurons. *J. Comput. Neurosci.* *7*, 5–15.
- Moczydlowski, E., and Latorre, R. (1983). Gating kinetics of Ca^{2+} -activated K^+ channels from rat muscle incorporated into planar lipid bilayers. *J. Gen. Physiol.* *82*, 511–542.
- Ozawa, S., Tsuzuki, K., Iino, M., Ogura, A., and Kudo, Y. (1989). Three types of voltage-dependent calcium current in cultured rat hippocampal neurons. *Brain Res.* *495*, 329–336.
- Poirazi, P., Brannon, T.M., and Mel, B.W. (2003). Arithmetic of subthreshold synaptic summation in a model CA1 pyramidal cell. *Neuron* *37*, *bxs-*bxs.
- Sah, P., and Bekkers, J.M. (1996). Apical dendritic location of slow afterhyperpolarization current in hippocampal pyramidal neurons: implications for the integration of long-term potentiation. *J. Neurosci.* *16*, 4537–4542.
- Spruston, N., Schiller, Y., Stuart, G., and Sakmann, B. (1995). Activity-dependent action potential invasion and calcium influx into hippocampal CA1 dendrites. *Science* *286*, 297–300.
- Stuart, G., and Spruston, N. (1998). Determinants of voltage attenuation in neocortical pyramidal neuron dendrites. *J. Neurosci.* *18*, 3501–10.
- Stuart, G., Spruston, N., Sakmann, B., and Hausser, M. (1997). Action potential initiation and backpropagation in neurons of the mammalian CNS. *Trends Neurosci.* *20*, 125–131.